Contents lists available at ScienceDirect

Materials Today Bio

A sequential macrophage activation strategy for bone regeneration: A micro/nano strontium-releasing composite scaffold loaded with lipopolysaccharide

Jinhui Huang [a,b], Jiawei Wei [b], Xue Xia [b], Shiqi Xiao [b], Shue Jin [b], Qin Zou [b], Yi Zuo [b], Yubao Li [b,**], Jidong Li [b,*]

[a] Yunnan Key Laboratory of Stomatology, School and Hospital of Stomatology, Kunming Medical University, Kunming, 650106, China
[b] Research Center for Nano-Biomaterials, Analytical & Testing Center, Sichuan University, Chengdu, 610064, China

ABSTRACT

Effective tissue repair relies on the orchestration of different macrophage phenotypes, both the M2 phenotype (promotes tissue repair) and M1 phenotype (pro-inflammatory) deserve attention. In this study, we propose a sequential immune activation strategy to mediate bone regeneration, by loading lipopolysaccharide (LPS) onto the surface of a strontium (Sr) ions -contained composite scaffold, which was fabricated by combining Sr-doped micro/nano-hydroxyapatite (HA) and dual degradable matrices of polycaprolactone (PCL) and poly (lactic-*co*-glycolic acid) (PLGA). Our strategy involves the sequential release of LPS to promote macrophage homing and induce the expression of the pro-inflammatory M1 phenotype, followed by the release of Sr ions to suppress inflammation. *In vitro* and *in vivo* experiments demonstrated that, the appropriate pro-inflammatory effects at the initial stage of implantation, along with the anti-inflammatory effects at the later stage, as well as the structural stability of the scaffolds conferred by the composition, can synergistically promote the regeneration and repair of bone defects.

1. Introduction

The immune response plays a crucial role in the healing process following tissue injury, influencing the speed and outcome of tissue regeneration and functional recovery [1–3]. In response, manipulating immune responses through biomaterial-associated strategies has emerged as an attractive approach in regenerative medicine [4,5].

The monocyte/macrophage system serves as the primary regulator of the immune response [6,7]. In response to tissue injury, monocytes are rapidly recruited to the injury site and undergo differentiation into macrophages [8]. These macrophages exhibit remarkable plasticity, allowing them to respond effectively to environmental signals and adjust their phenotype accordingly [9]. Typically, within approximately one week after injury, macrophages display a pro-inflammatory phenotype (M1), aiding in the clearance of damage-associated and pathogen-associated molecular patterns. Subsequently, there is a gradual transition of macrophages from the M1 to the M2 phenotype, with M2 macrophages promoting tissue repair [5,10]. The

pro-inflammatory M1 macrophages are crucial for initiating the healing process, while tissue healing requires the polarization of macrophages to the pro-regenerative M2 phenotype [3,11]. While the recruitment of macrophages to injury sites and their transition from the M1 to M2 phenotype occur naturally [10], However, for large-scale injuries requiring scaffold implantation to assist the healing process, cell infiltration, including macrophages, can be challenging due to the lack of blood vessels and nutrients. Therefore, artificial intervention to promote the transition of macrophage phenotype could enhance the healing process [12,13].

Based on the above points, this study proposes a hypothesis for scaffolds designed for immunomodulatory bone regeneration: they should be able to recruit macrophages in the early stage to clear injury-related molecules or pathogens, relying on pro-inflammatory M1 macrophages. Subsequently, when macrophages come into contact with the scaffold material, they should be able to quickly polarize into a pro-regenerative M2 phenotype to mediate tissue regeneration. Therefore, an ideal immunomodulatory biomaterial model should integrate pro-

---

inflammatory functions in the early stage with a pro-regenerative effect in the late stage. The *in vitro* feasibility of this model has been preliminarily demonstrated by Tan et al. [14]. They explored the response of macrophages to titanium dioxide nanotubes loaded with lipopolysaccharide (LPS), and showed that owing to the pro-inflammatory properties of LPS and the pro-regenerative properties of titanium dioxide, the inflammatory genes of macrophages first increased and then decreased *in vitro*. However, the *in vivo* effectiveness of such a model in bone repair scaffolds remains unclear, and its feasibility needs further verification. In particular, the selection of pro-inflammatory and anti-inflammatory factors and the concerted application of scaffold materials must be explored further [3,15].

Porous scaffolds, composed of inorganic hydroxyapatite (HA) and organic degradable polymers, are considered promising candidates for immunomodulatory bone regeneration, as they have been shown to be effective in bone regeneration [16,17]. The degradability of a scaffold can be a critical factor affecting osteogenesis. Our previous studies explored the effect of scaffold degradability on osteogenesis using three HA/polymer scaffolds and concluded that an ideal scaffold should achieve a balance between maintaining structural integrity and degradation rate [18,19]. Obviously, balancing degradation and structural integrity is challenging when using a single polymer. Therefore, employing two or more polymers with different degradation rates as the matrix material of a porous scaffold may facilitate achieving this balance. For example, one polymer with a faster degradation rate (e.g., PLGA, with a *in vivo* degradation time of several months) could degrade quickly to create space and facilitate the release of necessary elements for bone ingrowth, while another polymer with slower degradation (e.g., PCL, with a *in vivo* degradation time of 1–2 years) could maintain structural integrity. In recent years, researchers have developed several scaffolds with a dual matrix of PCL/PLGA to address this challenge [20, 21]. These studies have demonstrated the feasibility of the PCL/PLGA dual-matrix scaffold model.

When comparing different hydroxyapatite (HA) morphologies used to reinforce the polymer matrix, HA whiskers with higher aspect ratios have been shown to improve the mechanical strength of scaffolds more effectively than HA microspheres or particles, although this depends mainly on the degree of dispersion [22,23]. In a previous study, we developed strontium-doped ultralong HA whiskers (SrHAW) [24],

which can be used to synergistically reinforce a polymer matrix with Sr-doped nano-HA (n-SrHA) to construct a carrier scaffold for immunomodulatory bone regeneration. Here, Sr ions can be used to regulate the polarization of macrophages towards the anti-inflammatory M2 phenotype, as well as an active component of osteogenesis, because previous studies have reported that Sr ions can enhance the differentiation of bone marrow mesenchymal stem cells (BMSCs) into osteoblasts, alleviate osteoclast activity, and facilitate angiogenesis by regulating macrophage phenotype [25–27].

In this study, as diagramed in Fig. 1, strontium-doped ultralong HA whiskers (SrHAW) and strontium-doped nano-HA (n-SrHA) were synthesized and combined with PCL/PLGA dual matrices to prepare a composite porous scaffold (SHPP) with improved mechanical properties. Additionally, lipopolysaccharide (LPS) was physically adsorbed onto the SHPP composite scaffold to construct an SHPP/LPS scaffold. It is anticipated that LPS will be rapidly released after implantation to promote macrophage homing in defects and induce the pro-inflammatory M1 phenotype [28], thus facilitating immune clearance. Subsequently, with the effect of Sr ions, macrophages could gradually polarize into the M2 phenotype, promoting tissue repair. The immunoregulatory, angiogenic, and osteogenic effects of the SHPP/LPS scaffold were investigated to explore the feasibility of the new sequential immunomodulatory biomaterial model for bone regeneration.

2. Materials and methods

2.1. Reagents

PCL (MW = 80 kDa) was purchased from Shenzhen Esun Industrial Co., Ltd., China. PLGA (75:25, MW = 93 kDa) was purchased from Jinan Daigang Biological Materials Co., LTD, China. L-glutamic acid (L-Glu) and strontium chloride hexahydrate ($SrCl_2 \bullet 6H_2O$) were purchased from Meilun Biological Co., LTD, China. Other inorganic raw materials were of AR grade and purchased from Chengdu Kelong Chemical Co., LTD, China.
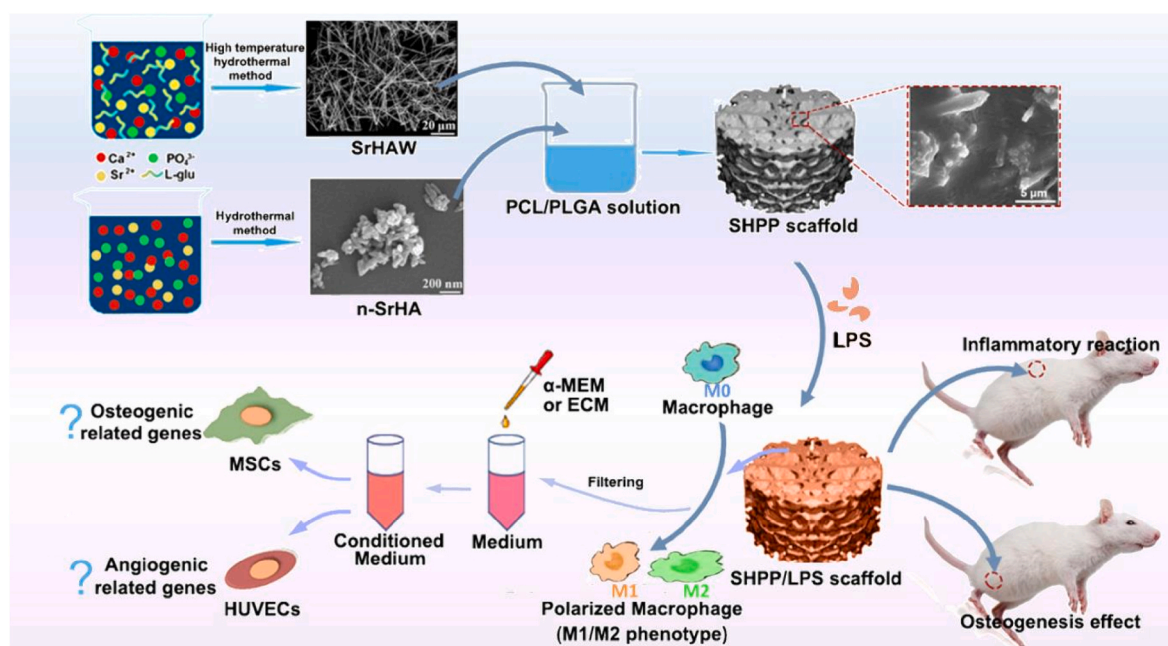

Fig. 1. Synthesis of SHPP/LPS composite scaffold and evaluation of its immune-mediated angiogenesis and osteogenesis *in vitro* and *in vivo*.

2.2. Synthesis and characterization of strontium-doped hydroxyapatite whiskers (SrHAW) and nanoparticles (n-SrHA)

SrHAW was synthesized using a bi-solvent (ethanol and water) system that we developed previously [24], where L-Glu was employed as a template and the molar ratio of Sr/(Sr + Ca) in the solution was controlled at 0.1. A wet chemical method without further sintering was used to fabricate n-SrHA, and the molar ratio of Sr to (Sr + Ca) in the solution was 0.1. The synthesis methods for SrHAW and n-SrHA are detailed in the Supplementary Information (SI).

The morphologies of the SrHAW and n-SrHA were observed using scanning electron microscopy (SEM, JSM-6510LV, Japan). The components and crystalline nature of SrHAW and n-SrHA were characterized by X-ray diffraction (XRD, DX2500, China) (with Cu Ka radiation at 40 kV and 25 mA). Transmission electron microscopy (TEM, Tecnai G2 F20 STWIN, USA) and energy dispersive spectroscopy (EDS, X-MaxN 20, Oxford, UK) were used to further investigate the crystallization state and Sr content of SrHAW.

2.3. Fabrication of porous scaffolds with different SrHAW/n-SrHA proportions

To investigate the effect of the n-SrHA/SrHAW ratio on the performance of the porous scaffolds, SrHAW and n-SrHA were combined into a PCL/PLGA matrix at different proportions, and then porous scaffolds were prepared using the particle leaching method [29]. To investigate the effect of the combination of PCL and PLGA and the introduction of Sr element on the scaffold performance, n-HA/PCL and n-HA/PCL/PLGA scaffolds were prepared for comparison. The abbreviations and formulae for the scaffolds are listed in Table 1.

2.4. Physicochemical characterization of the composite scaffolds

The morphologies of the scaffolds were observed by SEM, and the composition and elemental distribution in the scaffold were measured via EDS. The porosity of the scaffolds was determined in a gravity bottle using the ethanol immersion method [18].

The compressive strength and modulus of the scaffolds were evaluated using a universal mechanical testing machine (Autograph AG-IC 20/50 KN, Japan) according to the ASTM 5024-95 standard. The size of scaffolds for test was $\Phi 10$ mm $\times$ 10 mm, the compression head speed was 0.5 mm/min, the stress when the deformation reached 40 % of the original length was considered as the compressive strength of the scaffold, and the experiment was performed in quintuplicate.

2.5. Degradation assay in vitro

The porous scaffolds ($\Phi 6$ mm $\times$ 5 mm) were immersed in 5 mL PE tubes containing 4 mL deionized water, respectively, and placed in an oscillating chamber (37 °C) with a frequency of 2 Hz. Each group contained five parallel samples at each time point. The mass of the remaining scaffold and the pH value of the degradation solution were recorded at t weeks ($t = 0, 1, 4, 8, 12, 24$ weeks), and the concentrations of Ca and Sr in the degradation solution were measured by ICP-OES (Spectro, Germany). The relative residual mass M_R was calculated using the following formula:

$$M_R = \frac{M_t}{M_0} \times 100\%$$

where W_0 is the initial mass of the scaffold before the degradation test and M_t is the mass of the scaffold after degradation for t weeks.

The compressive strength and compressive modulus of scaffolds ($\Phi 10$ mm $\times$ 10 mm) after 12 weeks degradation was tested to assess the effect of degradation on the mechanical strength changes.

2.6. LPS loading and release of scaffold

The optimized SrHAW-incorporated composite scaffold was named SHPP and selected for LPS loading by comparing its compressive properties. Briefly, 10, 20, and 50 µg/mL LPS solutions were prepared with deionized water. The SHPP scaffolds were immersed in the above three LPS solutions, and the containers were placed in a vacuum drying oven. The internal pressure of the drying oven was adjusted to be less than 0.08 MPa and maintained for 20 min to ensure that the pores of the scaffold were filled with LPS solution. Thereafter, SHPP scaffold filled with LPS solution was placed in a −80 °C refrigerator for 1 h. Finally, SHPP scaffolds with different LPS loading were obtained by freeze-drying, and named as SHPP/LPS, SHPP/LPS20, and SHPP/LPS50 scaffolds according to the concentration of immersed LPS solution.

For detecting LPS release, place a SHPP/LPS scaffold ($\Phi 14$ mm $\times$ 1 mm) in a 50 mL centrifuge tube, add 20 mL of bacterial endotoxin detection water to each tube, and conduct the LPS release test in a 37 °C constant temperature shaker. At 1, 2, 4, 8, 12, 24, 36,48, and 72 h later, take 100 µL of the released liquid for detection, then supplement with 100 µL of bacterial endotoxin detection water in the tube. This experiment uses a chromogenic matrix limulus amebocyte lysate (LAL) kit to detect the amount of LPS released, and the specific steps are referred to the manufacturer's instructions (Beyotime, China). Cumulative release amount and cumulative release rate were calculated and curved, 3 parallel samples at each time point.

2.7. Cell culture

Rat-derived bone marrow mesenchymal stem cells (MSCs), mouse-derived macrophages RAW 264.7, and human umbilical vein endothelial cells (HUVECs) were used for *in vitro* studies. The details of MSCs extraction and culture refers to previous research [18]. RAW 264.7, obtained from West China Hospital of Sichuan University, were cultured in DMEM medium (Invitrogen, America) containing 10 % fetal bovine serum (FBS, Invitrogen, America). HUVECs, also obtained from the West China Hospital of Sichuan University, were cultured in ECM medium (Invitrogen, America) containing 5 % FBS and 1 % endothelial cell growth supplement/heparin kit (ECGS/H, PromoCell, Germany). All the above three types of cells were cultured in a 37 °C incubator with 95 % humidity and 5 % CO_2.

2.8. Evaluation of cytocompatibility of scaffolds

The scaffolds were cut into circular pieces ($\Phi 14$ mm $\times$ 1.5 mm) and γ-ray sterilized prior to evaluate their cytocompatibility. The 3rd passage MSCs were seeded onto the scaffolds at 2×10^4 cells/well in 24-well plates. The morphology of the MSCs on the scaffolds was observed using SEM. The proliferation of MSCs on the scaffolds was evaluated using a CCK-8 assay (KGA317S-500, KeyGEN, China) with a multilabel counter (Wallac Victor3 1420, PerkinElmer Co.) at 450 nm. A tissue culture plate without the scaffold was used as the blank control.

Table 1
Abbreviation and formula of scaffolds (wt%).

	n-HA	SrHAW	n-SrHA	PCL	PLGA
n-HA/PCL	30	0	0	70	0
n-HA/PCL/PLGA	30	0	0	50	20
SHPP-0	0	0	30	50	20
SHPP-1	0	10	20	50	20
SHPP-1.5	0	15	15	50	20
SHPP-2	0	20	10	50	20

2.9. Evaluation of macrophage phenotypes regulation

2.9.1. Morphology of RAW 264.7 cells on scaffolds

The scaffold was placed in a 24-well plate, and the RAW 264.7 cells were seeded on the scaffolds at 5×10^4 cells/well and co-cultured for 1 d. To investigate the effect of the scaffold on the morphology of macrophages, the morphology of RAW 264.7 cells on the scaffold was observed by SEM.

2.9.2. Immunofluorescence analysis of macrophage phenotypes

For the scaffold groups, 2 mL of the scaffold extract prepared with DMEM complete medium (according to GB/T 16886-11, scaffold surface area/medium = 3 cm^2/mL) was injected into 6-well plates with cell slides. For the Control group, 2 mL of complete normal DMEM was added. Next, 1 mL of RAW 264.7 cells suspension (1×10^5 cells/mL) was added to each well.

After culturing for 1 d, the supernatant was collected and filtered through a sterile filter, Subsequently, macrophage conditioning medium (CondM) of scaffold was prepared by mixed the supernatant with the corresponding scaffold extract prepared with ECM or α-MEM complete medium, at 1:1, for the later culture of HUVECs or MSCs cells. The CondM of the corresponding scaffold or control was abbreviated as n-HA/PCL/PLGA + CondM, n-SrHA/PCL/PLGA + CondM, SHPP + CondM, SHPP/LPS + CondM, and Control + CondM.

The phenotypes of RAW 264.7 cells cultured in the scaffold extract for 1 d were identified by immunofluorescence staining of CD206 and inducible nitric oxide synthase and observed by laser confocal microscopy (CLSM, NIKON Eclipse Ti, Japan) (blue for nucleus, stained by DAPI, with emission wavelength of 420 nm; green for CD206, as shown by FITC, with emission wavelength of 515–555 nm; red for iNOS, as shown by CY3, with emission wavelength of 590 nm). Fluorescence intensity was calculated using the ImageJ software.

2.10. Expression of angiogenic factors of HUVECs in macrophage conditioned medium

The expression of platelet-endothelial cell adhesion molecule (CD31) in HUVECs cultured in macrophage-conditioned medium was detected by immunofluorescence staining according to the manufacturer's protocol (Servicebio), and nuclei were stained with DAPI (Servicebio). The stained HUVECs were observed by CLSM (Blue for nucleus, stained by DAPI, emission wavelength 420 nm. Red for CD31, showed by CY3, emission wavelength 590 nm). The fluorescence intensity was calculated using Image J software.

The mRNA expression of angiogenesis related genes (FGF-2, Angiogen, VEGF and Ang1) was detected by real-time quantitative polymerase chain reaction (RT-qPCR). The extract of the SHPP scaffold without macrophage intervention is denoted as SHPP. Briefly, after removing the medium, the cells were washed three times with PBS, 5 min each. Total RNA was extracted using an RNA extraction kit (Servicebio, China) according to the manufacturer's instructions. Total RNA was reverse transcribed to obtain complementary DNA (cDNA). The target gene was amplified using PCR. The gene expressions were calculated by the $2^{-\Delta\Delta Ct}$ method. GAPDH was used as the internal reference, and the primer sequences for the internal reference and target genes are listed in Table S1.

2.11. Expression of osteogenic related genes in MSCs in macrophage conditioned medium

The mRNA expression of osteogenesis-related genes (BMP-2 and OCN) was also detected by RT-qPCR to investigate the effects of macrophages conditioned medium on promoting the osteogenic differentiation of MSCs. The process of RT-qPCR refers section 2.10, β-actin was set as the internal reference, and the primers of osteogenic genes were shown in Table S2. Before RT-qPCR test, the MSCs were inoculated with conditioned medium for 10 d.

2.12. Evaluation of inflammatory response in subcutaneous implantation

The scaffolds were cut into circular pieces with the size of Φ5 mm × 1 mm, sterilized by γ ray irradiation and subcutaneously implanted respectively into SD rats of approximately 300 g. Four parallel samples were set for each sample at each time point. Further, the wound directly sutured without implanting scaffold were set as blank control. The implanted scaffolds, together with the surrounding skin tissue, were harvested from the sacrificed animals 1 and 2 week(s) post-surgery. All animal experiments were approved by the Ethics Committee of West China Hospital of Sichuan University (2020264A). The fixed samples were paraffin-embedded and sectioned for H&E staining and immunohistochemical (IHC) staining of CD163 (a marker of M2 macrophages) and iNOS (a marker of M1 macrophages) according to the manufacturer's instructions. Finally, stained sections were observed and photographed under a light microscope (TE 2000-U; Nikon, Tokyo, Japan).

2.13. Evaluation of in vivo osteogenesis

The scaffolds were cut into columns measuring Φ5 mm × 4 mm, and sterilized by γ ray irradiation. A defect of Φ 5 mm × 4 mm was drilled in the medial condyle of the femur at SD rats of approximately 300 g. The scaffolds were implanted into the defects and the wounds were sutured. Five parallel samples were set for each sample at each time point, and defects directly sutured without implanting scaffold were set as blank control. Femoral condyles were harvested at 4 and 12 weeks postoperatively and fixed with 4 % paraformaldehyde for 1 week for micro-CT or histological section analysis. All animal experiments were approved by the Ethics Committee of West China Hospital of Sichuan University (2020264A).

2.13.1. Reconstruction of new bone by micro-CT

Harvested femoral condyles were scanned, reconstructed, and quantitatively analyzed using micro-CT (Scanco Medical, Bru Ttisellen, Switzerland). A threshold of 220–1000 was used to distinguish bone tissue from scaffold material. A circular region of interest (ROI) of Φ5 mm was selected in the implantation area and a three-dimensional (3D) reconstructed image of the new bone tissue was obtained from 100 axial images. The bone volume to total volume ratio (BV/TV), trabecular thickness (Tb.Th) and trabecular separation (Tb.Sp) was calculated using the software attached to the micro-CT according to the 3D reconstructed images.

2.13.2. H&E staining of bone tissue

The fixed bone tissues were decalcified, paraffin-embedded, and sectioned for H&E staining, according to the manufacturer's instructions. Finally, the stained sections were observed and photographed under a light microscope.

2.14. Statistical analysis

Quantitative data were expressed as mean ± standard deviation (SD), and Student's t-test was performed to assess statistical significance using SPASS software. Differences were considered significant at P < 0.05.

3. Results and discussion

3.1. Morphology and composition of SrHAW and n-SrHA

SEM images (Fig. 2A and B) revealed that the Sr-doped HA whiskers (SrHAW) were approximately 50–80 μm in length and 0.5–1 μm in diameter. The Sr-doped nano HA (n-SrHA) appeared as short rods, with most rods measuring 70–100 nm in length and 10–20 nm in diameter.
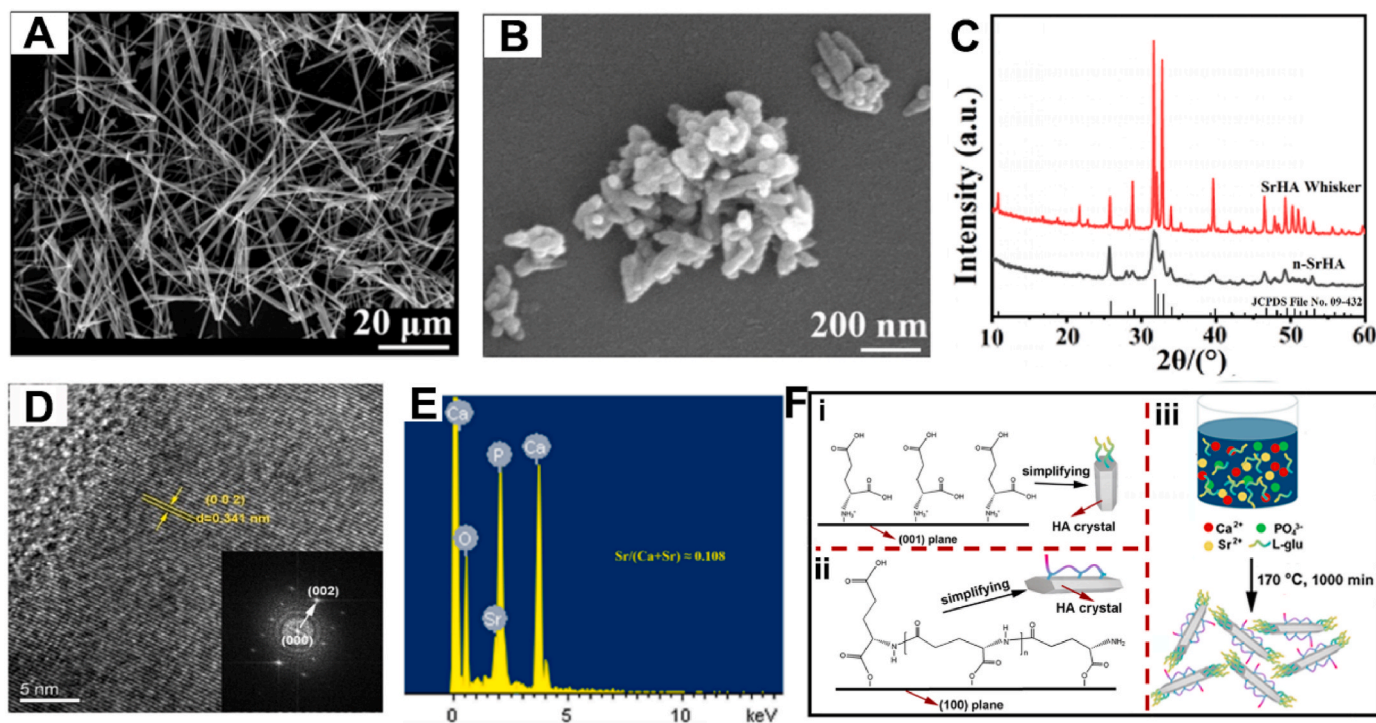
Fig. 2. Micro/nano Sr-dopped HA for scaffolds. SEM images of SrHAW (A) and n-SrHA (B); XRD patterns of SrHAW and n-SrHA (C); HRTEM image and SAED pattern (inset) of SrHAW(D); EDS elemental analysis of SrHAW (E); Schematic process for the formation of SrHAW crystals (F).

Both types of Sr-doped HA exhibited uniform size distributions suitable for reinforcing the polymer matrix. XRD patterns (Fig. 2C) showed peaks consistent with standard HA samples (JCPDS No.09-0432), with differences in peak intensity. SrHAW exhibited significantly higher peak intensity than n-SrHA, likely due to its larger crystal size and higher crystallinity.

The results of the crystal plane spacing (in Fig. 2D, the crystal plane spacing of the (0 0 2) plane is 0.341 nm) and the SAED pattern (inset in Fig. 2D) showed that each whisker of SrHAW was an HA single crystal. High crystallinity always implies fewer defects; therefore, the single-crystal structure may be helpful for SrHAW to maintain its structural stability such that it served more effectively as a reinforcing phase. SrHAW and n-SrHA possessed almost the same EDS spectra and similar Sr/(Sr + Ca); thus, herein, only the results of SrHAW are selectively shown. The EDS spectrum (Fig. 2E) indicates the presence of Sr, and the molar ratio of Sr/(Sr + Ca) was approximately 0.108, which is close to preset one.

Our previous study presented the mechanism for the formation of ultralong whiskers [24]. In conclusion, there are two adsorption modes of L-glu on HA surface. One is, as shown in Fig. 2Fi, the amino group of L-glu adsorbed directly onto the (0 0 1) plane of HA, and the linkage between adjacent L-glu barely occurred. Another is, as shown in Fig. 2Fii, the carboxyl group adjacent to the α-site carbon adsorbs to the (1 0 0) plane of HA, the free amino group can couple the free carboxyl group of adjacent L-glu to form the C–N–C layered structure on (1 0 0) plane. The relatively free adsorption model was easier to adsorb and desorb than the layered structure, thus the adsorption/desorption behavior of L-glu on (0 0 1) plane was more frequent and easier than that occurring on (1 0 0) plane. Consequently, as shown in Fig. 2Fiii, HA crystal grew along the c-axis and formed whiskers.

3.2. Optimization of the SrHAW and n-SrHA composite proportion in the scaffolds

Fig. 3A and B shows the porous structures of SrHAW- and n-SrHA-reinforced PCL/PLGA composite scaffolds. As evident, the size of most large pores in the scaffold ranged as 250–550 μm, and the large pores connected with each other through little pores to ensure the penetrability of the porous scaffolds. The porosities of the scaffolds with different ratios of SrHAW and n-SrHA were similar and greater than 70 % (Fig. 3C). The rough surface structure of the scaffolds was conducive to the adsorption of proteins and attachment of cells, and the highly permeable pore structure and high porosity were suitable for the growth of new bone tissue into the scaffolds as well as for the transportation of oxygen and nutrients [30,31]. Fig. 3D and G shows the compressive strength and modulus of the composite scaffolds, respectively. Compared with the n-HA/PCL scaffold, after 2/7 of PCL was replaced with PLGA, the compressive strength of the SHPP-0 scaffold did not change significantly; However, the compressive modulus was significantly improved. After the SrHAW whiskers were incorporated, the compressive strength and modulus of the scaffolds significantly improved, and the SHPP-1.5 scaffold exhibited the highest compressive strength and modulus. With a further increase in the SrHAW ratio, the modulus of the SHPP-2 scaffold was similar with that of the SHPP-1.5, whereas the strength of SHPP-2 decreased significantly. The amplified SEM images showed that the whiskers (SrHAW) in the SHPP-1.5 scaffold were uniformly dispersed and anchored in the polymer matrix (Fig. 3E and F), indicating that SrHAW played a role in strengthening the polymer matrix. The whiskers play roles in enhancing the polymer matrix through four mechanisms, including crack deflection, crack bridge link, whisker pullout and microcrack propagation. For more details, please refer to previous research [32].

Whereas, agglomeration of SrHAW was observed in SHPP-2 (Fig. 3H and I), SrHAW was not evenly distributed in nor fully trapped by the polymer matrix, which explains why the compressive strength of the SHPP-2 scaffold was inferior to that of the SHPP-1.5 scaffold. Therefore, the SHPP-1.5 scaffold was selected for subsequent studies and is abbreviated as the SHPP scaffold.

The EDS spectrum (Fig. 3J) of the SHPP scaffold shows that the main elements in the scaffold, including C, O, Ca, P, and Sr, were consistent with those of the raw materials. The Sr/(Sr + Ca) ratio calculated from EDS results was approximately 0.083, lower than that in SrHAW and n-
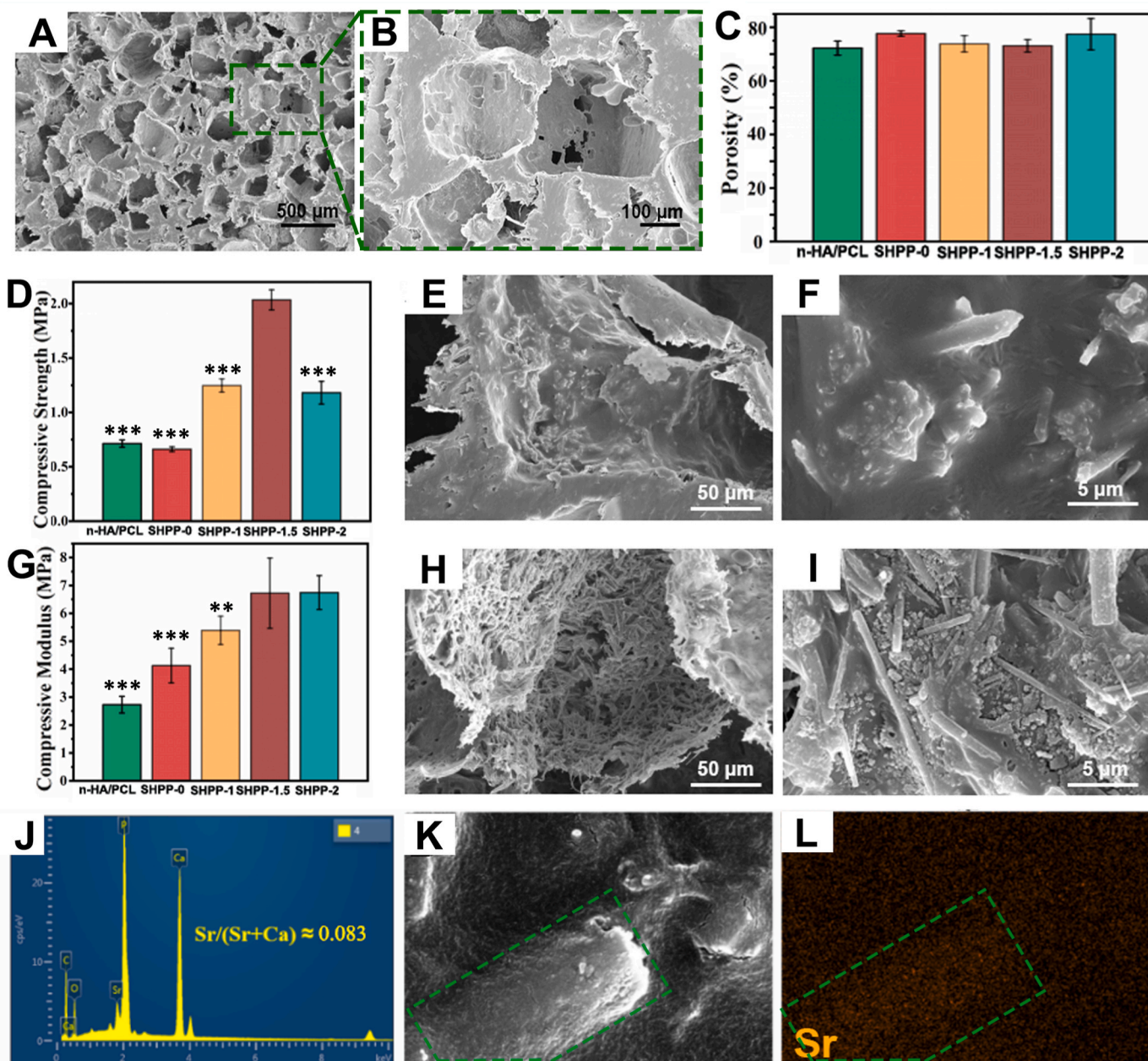
Fig. 3. Porous structure (A, B), porosity (C), compressive strength (D) and compressive modulus (G) of scaffolds; SEM images of whisker distribution in scaffolds: SHPP-1.5 scaffold (E, F); SHPP-2 scaffold (H, I); EDS analysis (J), electronic image (K) and element distribution (L) of SHPP-1.5 scaffold. * represents comparing with SHPP-1.5, *$P < 0.05$, **$P < 0.01$, ***$P < 0.001$.

SrHA, also lower than true overall value in the scaffold. The direct reason was that, EDS detected elemental signals 1 μm deep on the scaffold material surface, while the dissolution loss ratio of Sr ions on the surface of the scaffold was higher than that of Ca during removing pore-forming agent. A deeper reason is that, compared with the relatively perfect crystal structure of standard HA, partially Sr-doped HA is more prone to crystal defects [33]. Thus, it is more prone to dissolution and ionization, resulting in a lower ratio of Sr/(Sr + Ca) in the remaining crystals. Fig. 3L shows that Sr is composed of two parts: one originates from SrHAW (denoted by the green dotted box), and the other from n-SrHA dispersed uniformly in the scaffold.
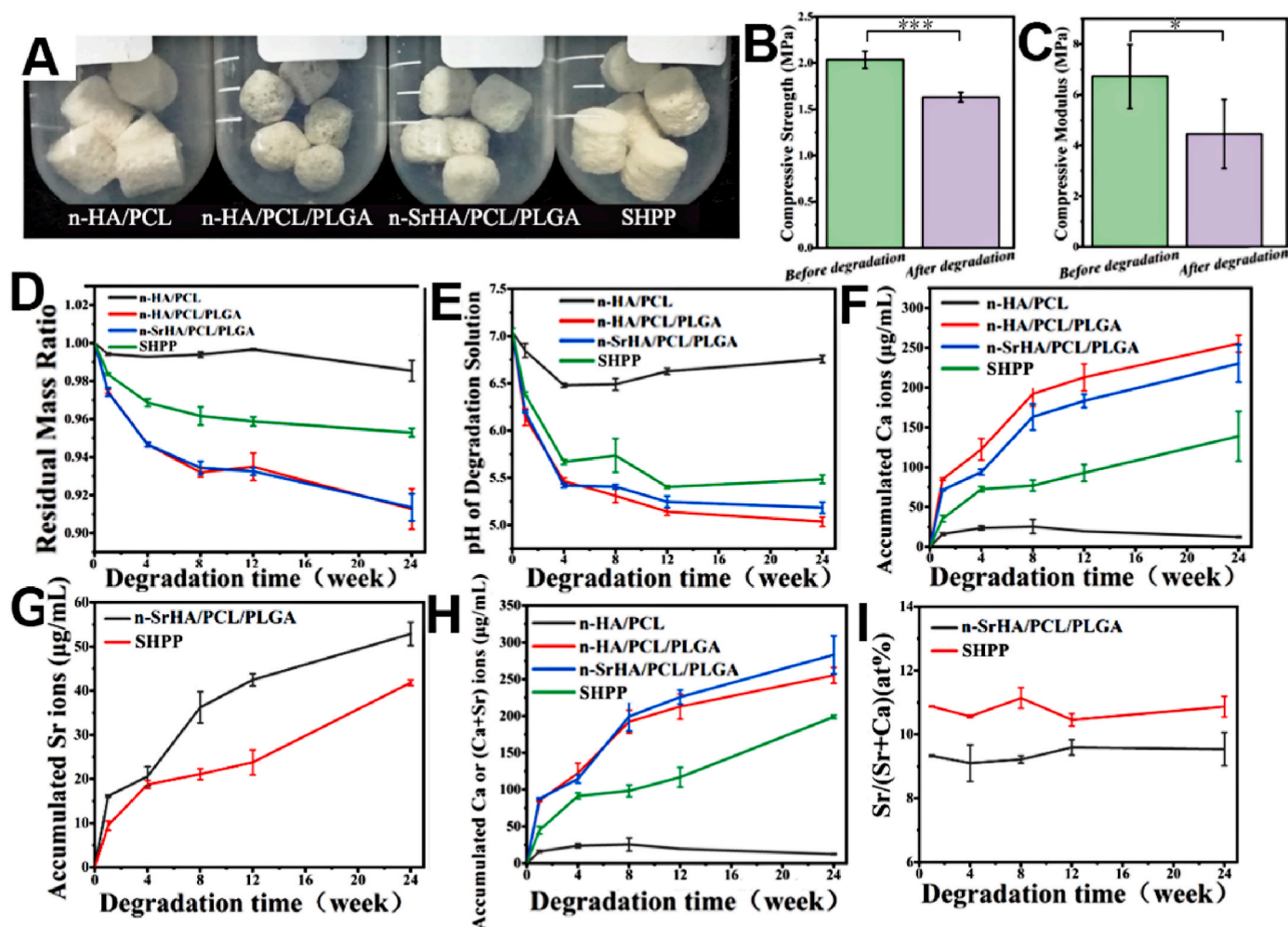
3.3. In vitro degradation of scaffolds and release of Ca and Sr ions

Fig. 4 shows the *in vitro* degradation results of the scaffolds. The degradation of the SHPP scaffolds gradually slowed over 24 weeks. This is because the proportion of PLGA in the scaffold was relatively high at the beginning; therefore, a relatively fast degradation rate was observed in the early stage. The degradation rate flattened as the proportion of PLGA decreased. After 12 weeks of degradation, both the compressive strength and modulus of the SHPP scaffold decreased by approximately 25 % and 33 %, respectively (Fig. 4B and C), which is mainly attributed to the increase in vacancies caused by degradation in the scaffold. However, such a decrease would not cause structural collapse. In addition, this gradual decrease in compressive strength may expose new bone tissue to increased force stimulation, thus promoting the bearing capacity of the new bone tissue after implantation and accelerating bone regeneration and reconstruction [34,35].

To better understand the degradation behavior of the SHPP scaffold, the effects of SrHAW whisker incorporation on the degradation of the

Fig. 4. Degradation of scaffolds *in vitro*. (A) Digital photos of scaffolds after degradation for 12 weeks; Compressive strength (B) and compressive modulus (C) of SHPP scaffold before and after degradation for 12 weeks, n = 3, *P < 0.05, **P < 0.01, ***P < 0.001; Residual mass ratio curves of scaffolds (D); pH value change of degradation solution (E); Concentration curves of accumulated Ca ions (F), Sr ions (G), Ca or Ca + Sr ions (H) in degradation solution; Sr/(Sr + Ca) ratio curves of degradation solution (I).

SHPP scaffold, PCL single-matrix scaffold (n-HA/PCL scaffold), and dual-matrix scaffolds without SrHAW (n-HA/PCL/PLGA and n-SrHA/PCL/PLGA scaffolds) were used for comparison. The slowly degrading n-HA/PCL scaffold maintained its initial shape after 12 weeks of degradation (Fig. 4A), and almost no mass loss was observed after 24 weeks (<2 %, Fig. 4D). Consequently, changes in pH (Fig. 4E) and accumulated Ca ions (Fig. 4F) in the n-HA/PCL group were minor. The degradation behaviors of the n-HA/PCL/PLGA and n-SrHA/PCL/PLGA scaffolds were analogous. Under erosion of the aqueous solution, the overall size of the two scaffolds was reduced, and the original edges of the cylinder became more rounded (Fig. 4A). Further, their mass loss was the largest among all scaffolds (Fig. 4D), and the change in pH value and the concentration of Ca or (Ca + Sr) was also the highest. The SHPP scaffold maintained its structural integrity after 12 weeks of degradation (Fig. 4A). Its size and shape did not change significantly compared with the n-HA/PCL/PLGA and n-SrHA/PCL/PLGA scaffolds, and its appearance was indistinguishable from that of the n-HA/PCL scaffold. This phenomenon was mainly owing to the strengthening effect of the SrHAW whiskers, which effectively resisted the damage caused by solution erosion. However, compared to the n-HA/PCL scaffold, the SHPP scaffold exhibited significant degradation (Fig. 4D–I). The mass loss of the SHPP scaffold after 24 weeks was approximately half that of the n-HA/PCL/PLGA and n-SrHA/PCL/PLGA scaffolds (Fig. 4D). The pH value change trend of the SHPP group was consistent with the trend of the n-

HA/PCL/PLGA and n-SrHA/PCL/PLGA groups (Fig. 4E). The pH decreased rapidly in the first 4 weeks, and the decline leveled off in the subsequent 20 weeks. After 24 weeks, the pH of the SHPP group was approximately 5.5, and less acidic than those of the n-HA/PCL/PLGA and n-SrHA/PCL/PLGA groups. The accumulated ion concentration in the SHPP group exhibited a gradual upward trend (Fig. 4F–G). After 24 weeks of degradation, the accumulated Sr and (Ca + Sr) ion concentrations in the SHPP group were approximately 76 % and 64 %, respectively, of those in the n-SrHA/PCL/PLGA group. The Sr/(Ca + Sr) ratio in the degradation solution of the n-SrHA/PCL/PLGA and SHPP scaffolds was stable at approximately 9.5 % and 10.5 % (Fig. 4I), respectively, indicating the ratio of Sr to replace Ca in the HA of the two scaffolds (10 %).

The *in vitro* degradation study illustrates that, owing to the combination of dual-matrices, slow-degradable PCL, and fast-degradable PLGA, the SHPP scaffold possesses gradient degradability. During the 24 weeks degradation period, PCL in the SHPP scaffold remained stable and acted as a guardian to maintain structural integrity, whereas PLGA acted as the main degradation contributor. In addition, the degradation of inorganic particles (n-HA, n-SrHA, and SrHAW) in the dual-matrix scaffolds, which rarely occurred in the n-HA/PCL scaffold, was mainly driven by the weakly acidic environment created by PLGA degradation. This driving force promotes the sustained release of Ca and Sr ions, which play important roles in bone formation after implantation.

Furthermore, owing to the reinforcement and toughening effects of the SrHAW whiskers, the SHPP scaffold was more resistant to structural damage when subjected to solution erosion.

3.4. Adhesion and proliferation of MSCs on scaffolds

The cytocompatibility of the scaffolds was studied based on the adhesion and proliferation behaviors of MSCs on the scaffolds. SEM observations (Fig. 5A) showed that after 4 and 7 d of culture, MSCs (endowed with a green pseudocolor) spread well on the surface of all three scaffolds, exhibiting typical polygons of MSCs and abundant pseudopods. Specifically, the cells were in contact with each other through extensions of longer and more pseudopodia after 7 d. Benefitting from the partially exposed SrHAW whiskers, the SHPP scaffold provided more climbing sites for cells; therefore, MSCs presented a 3D climbing growth trend on the scaffolds after 4 d. CCK-8 results (Fig. 5B) showed that although the optical density (OD, reflecting relative cell quantity) of all the three scaffolds was lower than that of the control, a significant upward proliferation trend of MSCs was observed in all three scaffold groups for 1–7 d. Moreover, the OD value of each scaffold group was greater than 80 % of that of the control during all 7 days, and the

corresponding cytotoxicity grade is 1, indicating no significant cytotoxicity. These results suggest that all three scaffolds have good cytocompatibility and that the subsequent study schedule can run forward.

3.5. Regulation of macrophage polarization

Previous studies reported that Sr doping can promote early angiogenesis, owing to the role of Sr ions in regulating macrophage polarization into the M2 phenotype [27]. Pure PLGA scaffolds have been reported to be associated with stronger inflammatory responses [36]. To explore the effect of the composite scaffolds containing Sr ions and PLGA, we investigated the effects of n-HA/PCL/PLGA, n-SrHA/PCL/PLGA, and SHPP scaffolds on macrophage phenotype regulation. We also investigated macrophage response to the SHPP/LPS scaffold to explore whether the introduction of the pro-inflammatory active ingredient LPS would completely polarize macrophages into the M1 phenotype. Fig. 5C shows that the cells in the control group were spherical or ellipsoidal, with few short pseudopods, and in an unpolarized state. However, the cells in all the scaffold groups presented numerous longer pseudopods and were polarized to certain a degree. Previous studies have reported that, the macrophages of M1 phenotype
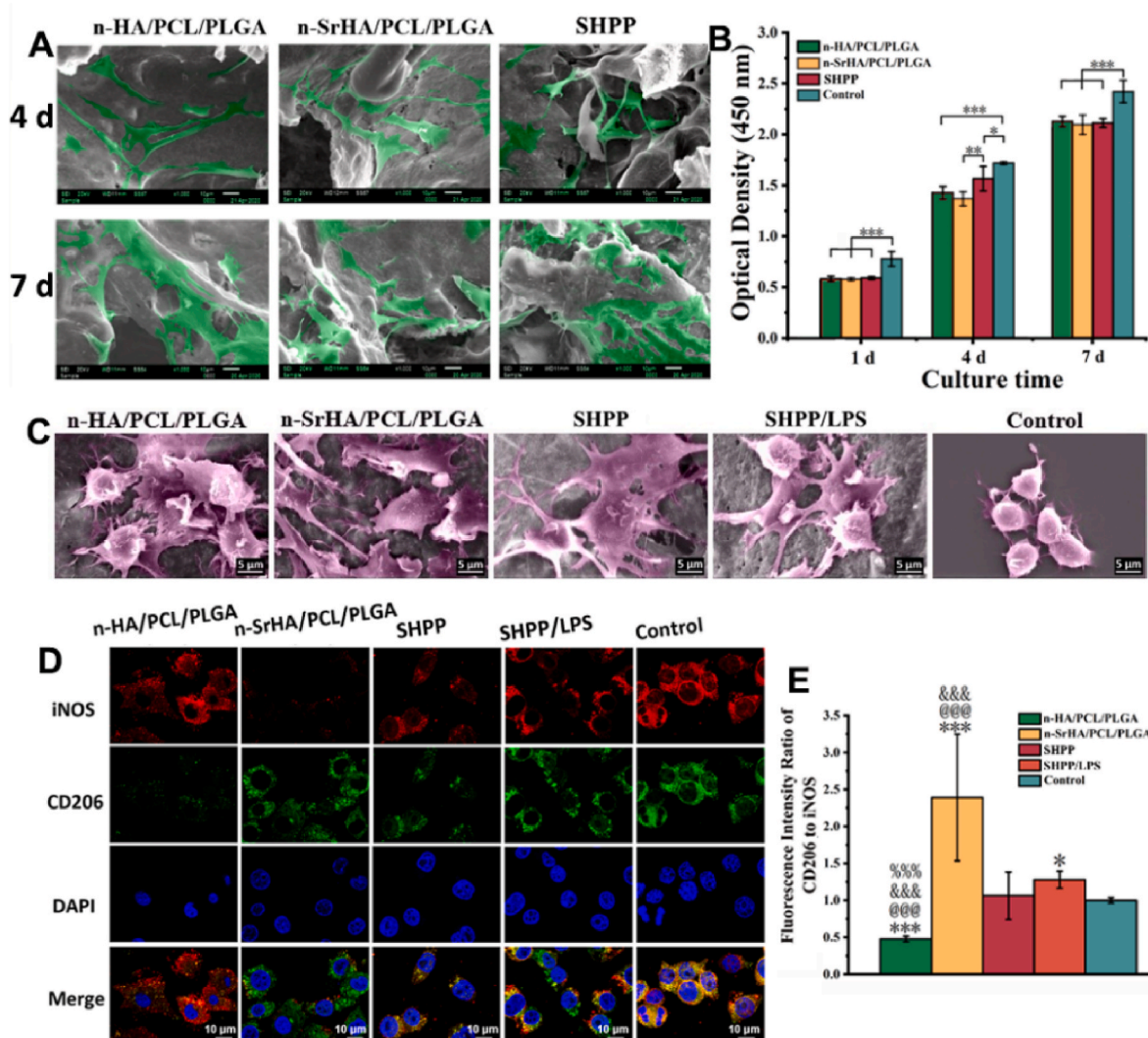

Fig. 5. Pseudocolor treated SEM images of MSCs cultured on the n-HA/PCL/PLGA, n-SrHA/PCL/PLGA and SHPP scaffolds (A); CCK-8 assay for cell proliferation of MSCs cultured with the scaffolds (B) (n = 3, *P < 0.05 , **P < 0.01 , ***P < 0.001); Pseudocolor treated SEM images of RAW 264.7 cells cultured on scaffolds for 1 day (C); Immunofluorescence staining images of RAW 264.7 cultured with the scaffold extract solution for 1 day (D) and the fluorescence intensity ratio of CD206 to iNOS that normalized to Control (E). * represents comparing with Control, @ represents comparing with SHPP/LPS, & represents comparing with SHPP, and % represents comparing with n-SrHA/PCL/PLGA. n = 3, take * as an example, *P < 0.05, **P < 0.01, ***P < 0.001.

were relatively spherical, while M2 phenotype were relatively elongated [37,38]. Accordingly, based on the results shown in Fig. 5C, it can be predicted that the n-SrHA/PCL/PLGA scaffold was more capable of polarizing macrophages towards M2 phenotype, whereas the n-HA/PCL/PLGA scaffold mainly polarizes macrophages towards M1 phenotype. The SHPP scaffold can polarize macrophages towards M2 phenotype to a certain extent; therefore, the cells on the SHPP/LPS scaffold were not completely spherical, despite LPS loading in the scaffold. LPS release curve from per cubic centimeter of SHPP/LPS scaffold was shown in Fig. S1. LPS released rapidly from scaffold within 8 h and slowed down at 12 h. At 72 h, the cumulative release of LPS in the scaffold was about 450 ng, and the cumulative release rate was about 90 %.

The immunofluorescence staining results (Fig. 5D) of RAW 264.7 macrophages, were consistent with the results from SEM. The expression levels of CD206 (a marker of M2 macrophages, green fluorescence) and iNOS (a marker of M1 macrophages, red fluorescence) in the control group were similar, and the images were yellow after merging. The n-SrHA/PCL/PLGA group polarized macrophages towards the anti-inflammatory M2 phenotype; thus, CD206 was highly expressed. The n-HA/PCL/PLGA group mainly promoted the polarization of macrophages into the pro-inflammatory M1 phenotype; therefore, iNOS was highly expressed in these cells. The results of the SHPP scaffold group did not exhibit a significant trend towards M2 phenotype, and the overall expression level was similar to that of the control group. Interestingly, although LPS was introduced, the overall expression of CD206 in the SHPP/LPS scaffold was slightly higher, and the fluorescence intensity ratio of CD206 to iNOS was higher than that in the control group ($P < 0.05$).

Macrophage polarization can be influenced by the chemical composition and physical properties of the scaffold [1,3,39]. As shown by the *in vitro* degradation results in Section 3.3, the overall degradation trends of n-HA/PCL/PLGA and n-SrHA/PCL/PLGA were similar, and the difference was in the release of Sr and Ca ions. The n-HA/PCL/PLGA scaffold or its extract induced the polarization of RAW 264.7 cells towards M1 phenotype, which is mainly dominated by the acidic product of scaffold PLGA, as pure PLGA scaffolds has been reported to be associated with a stronger inflammatory response [36]. In the n-SrHA/PCL/PLGA group, M2 phenotype polarization of RAW 264.7 cells were observed. This may be owing to the dominant position of Sr ions in the antagonism between Sr ions and PLGA acidic products, due to the key role of Sr ions in promoting M2 phenotypes of macrophages [27, 40]. Therefore, the presence of Sr ions in the SHPP scaffold antagonized the M1 phenotype polarization effect of macrophages induced by acid products compared with the n-HA/PCL/PLGA group. M2 phenotype polarization in the SHPP group was not as clear as that in the n-SrHA/PCL/PLGA group, which could be attributed to the lower Sr ion concentration released by the whiskers in the SHPP scaffold because the whiskers were highly crystalline. The effect of the SHPP scaffold on M2 polarization from immunofluorescence staining was not as obvious as that from SEM observation, which could be attributed to the different characterization processes in the two methods, one in culture with the extract (to avoid the interference of spontaneous fluorescence of materials) and one in direct contact with the scaffold. When scaffold extract is used, the cells are stimulated only by the degradation products in the extract. When the cells are directly cultured on the scaffold, they are affected by the released ions and degraded products as well as the chemical composition and physical properties of the scaffold itself. For instance, the higher rigidity of materials has been reported to promote the M2 phenotype polarization of macrophages [41,42]. In the SHPP scaffold, both the undissolved Sr-doped inorganic active ingredients and the higher rigidity (compressive modulus) of the SHPP scaffold compared to those of the n-SrHA/PCL/PLGA scaffold can stimulate the M2 phenotype polarization of macrophages. Therefore, in the SEM results, the SHPP scaffold exhibited a relatively obvious trend of promoting M2 polarization. In the real situation of scaffold implantation *in*

vivo, the degradation products and material matrix of the scaffold interact with cells together; therefore, the SEM result that the SHPP scaffold can promote macrophage polarization to M2 phenotype is credible. For the SHPP/LPS scaffold, macrophages showed the coexistence of anti-inflammatory and pro-inflammatory phenotypes, indicating that the presence of LPS did not completely polarize macrophages to the M1 phenotype, further illustrating that the SHPP scaffold has the potential to resist the polarization of macrophages into the M1 phenotype after LPS stimulation.

3.6. Effects of macrophage conditioned medium on the expression of angiogenic factors of HUVECs

Vascularization is essential for the growth of most tissues. For a long time, macrophages were considered to play a key regulatory role in angiogenesis [43–45]. In this section, the proangiogenic potential of macrophage-conditioned media from several scaffolds was explored. Immunofluorescence staining of CD31 in HUVECs (Fig. 6A and B) showed that, compared with the Control + CondM group, CD31 over-expression was observed in several scaffold macrophage-conditioned medium groups ($P < 0.05$). Specifically, the n-SrHA/PCL/PLGA + CondM group exhibited the highest expression of CD31, which was approximately twice that of the Control + CondM group. The expression of CD31 in the SHPP + CondM and SHPP/LPS + CondM groups was slightly lower than that in the n-SrHA/PCL/PLGA + CondM group and higher than that in the n-HA/PCL/PLGA + CondM group. In the SHPP group without macrophage intervention, almost no obvious expression of CD31 was observed, similar with the Control + CondM group. These results suggest that 1) the n-HA/PCL/PLGA, n-SrHA/PCL/PLGA, SHPP, and SHPP/LPS scaffolds may upregulate the expression of CD31 in HUVECs by activating macrophages to M1 or M2 phenotype, and 2) the higher the ability to polarize M2, the higher the expression of CD31.

The expression of angiogenesis-related genes in HUVECs, as determined by RT-qPCR (Fig. 6C), was consistent with the trend in CD31 expression. The n-SrHA/PCL/PLGA + CondM group exhibited the highest up-regulation expression of FGF-2, angiogenesis, VEGF, and Ang1 among all the groups ($P < 0.001$), which could be attributed to the effect of the scaffold on polarizing macrophages into M2 phenotype. Compared with the Control + CondM, there was no significant up-regulation of angiogenesis-related genes in the SHPP group ($P > 0.05$), whereas the SHPP + CondM group showed significant up-regulation of FGF-2, Angiogen and Ang1 expression ($P < 0.05$). This further confirmed that SHPP and n-SrHA/PCL/PLGA may promote angiogenesis indirectly by regulating the phenotypes of macrophages. The expression of FGF-2, Angiogenin and Ang1 in SHPP/LPS + CondM group was slightly downregulated compared with that in the SHPP + CondM group ($P < 0.05$), and the expression level of VEGF was similar to that in the SHPP + CondM group. In addition, the expression of Angiogenin, VEGF, and Ang1 in SHPP/LPS + CondM group was higher than that in the Control + CondM group ($P < 0.05$), suggesting that the changes in macrophage behavior induced by LPS can affect the cytokine expression of HUVECs. The expression of Angiogenin and FGF-2 in the n-HA/PCL/PLGA + CondM group was similar to that in the Control + CondM group ($P > 0.05$); however, its VEGF and Ang1 expression was significantly upregulated, and its VEGF level was comparable to the SHPP + CondM group. Moreover, Ang1 was significantly higher than that of the SHPP + CondM group ($P < 0.05$). The RT-qPCR results further indicated that both M1 and M2 phenotype polarization of macrophages induced by scaffold materials may upregulate the expression of angiogenesis-related factors in HUVECs; however, M2 polarization of macrophages exhibited a more significant promoting effect than M1 polarization.
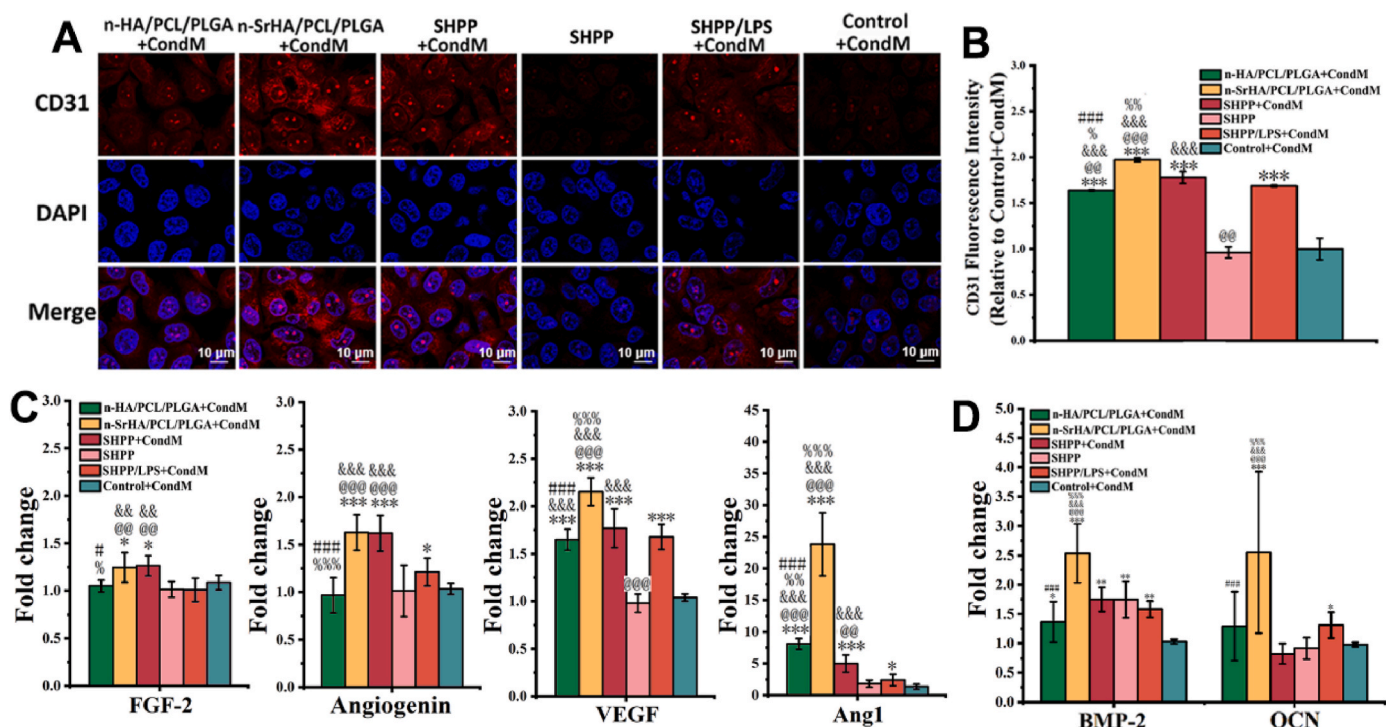
Fig. 6. CD31 immunofluorescence staining images (A) and semi-quantitative results of fluorescence intensity (B) of HUVECs cells cultured in macrophage conditioned culture medium for 7 days; The mRNA expressions of FGF-2, Angiogen, VEGF and Ang1 in HUVECs cells cultured in macrophage conditioned medium for 7 days (C); The mRNA expressions of BMP-2 and OCN in MSCs cells cultured in macrophage conditioned medium for 10 days (D). * represents comparing with Control + CondM, @ represents comparing with SHPP/LPS + CondM, & represents comparing with SHPP, % represents comparing with SHPP + CondM, # represents comparing with n-SrHA/PCL/PLGA. n = 3, take * as an example, *P < 0.05, **P < 0.01, ***P < 0.001.

3.7. Effects of macrophage conditioned medium on the expression of osteogenic factors of MSCs

To investigate whether macrophage-conditioned media have the potential to promote the osteogenic differentiation of MSCs, the expression of BMP-2 and OCN in MSCs after 10 d of culture was detected by RT-qPCR (Fig. 6D). The expressions of BMP-2 and OCN in the SHPP + CondM, SHPP, and SHPP/LPS + CondM groups were not significantly different. This indicated that the regulation of macrophage polarization by the scaffold had no significant effect on the expression of osteogenesis-related genes in MSCs and that the introduction of a small amount of LPS did not directly downregulate osteogenesis-related gene expression. The expression in the n-HA/PCL/PLGA + CondM group was not significantly different from that in the SHPP + CondM, SHPP, and SHPP/LPS + CondM groups, which may be explained by the difference in Ca and Sr ion concentrations in the extracts. Both Ca and Sr ions can affect the migration, proliferation, and differentiation of osteoblasts [46, 47]. However, studies have shown that the introduction of a small amount of Sr ions has a more significant osteogenic effect than Ca ions alone [48]. In the present study, the degradation of the SHPP scaffold and the release of ions were slower. The total Ca and Sr ion concentrations in the SHPP extract were lower than those in the n-HA/PCL/PLGA scaffold. Nevertheless, the stronger bone-promoting effect of Sr ions relative to Ca ions compensated for the lack of overall ion concentration in the SHPP scaffold; therefore, the expression of osteogenesis-related genes was not significantly different between the n-HA/PCL/PLGA + CondM and the SHPP + CondM, SHPP, and SHPP/LPS + CondM groups. The expression levels of BMP-2 and OCN in the n-SrHA/PCL/PLGA + CondM group were the highest among all groups, which could be attributed to the higher concentration of Ca and Sr ions in the extract compared with those in the SHPP group, wherein Sr ions played a more dominant role.

Although the angiogenesis and osteogenesis effects *in vitro* of the SHPP and SHPP/LPS scaffolds are indeed lower than those of the n-SrHA/PCL/PLGA scaffold, the *in vivo* implantation environment is always more complicated, which might accelerate the degradation of SHPP and SHPP/LPS scaffolds, thus increasing Sr ion release and improving the efficiency of angiogenesis and osteogenesis. Considering that the structural integrity and stability of the SHPP and SHPP/LPS scaffolds may be beneficial for tissue regeneration *in vivo*, it is necessary to compare the n-SrHA/PCL/PLGA, SHPP, and SHPP/LPS scaffolds through *in vivo* implantation experiments.

3.8. Immune response induced by the scaffold in subcutaneous implantation model

Material implantation is always accompanied by an immune response that determines the process and outcome of tissue repair [1, 49]. To evaluate the inflammatory response of the scaffolds, the material and surrounding tissues were histologically sectioned after subcutaneous implantation and stained with H&E and IHC.

The H&E staining results at 7 d (Fig. 7A) showed that the level of cell infiltration in the n-HA/PCL/PLGA, n-SrHA/PCL/PLGA, and SHPP scaffold groups was lower than that in the scaffold groups with LPS. The infiltrating cells in the scaffold group without LPS were concentrated at the edge of the scaffold, and fewer inflammatory cells were observed. With the introduction and concentration elevation of LPS, cells gradually penetrated the inner area of the scaffold in the SHPP/LPS, SHPP/LPS20, and SHPP/LPS50 groups, and the number of inflammatory cells also gradually increased. These results indicate that LPS plays an important role in recruiting cells to infiltrate in early, including inflammatory cells.

Neovascularization was observed in the implantation areas of all groups (The enlarged H&E images in Fig. 7A). The semi-quantitative results (Fig. 7B) showed that the relative vascular areas of the SHPP/LPS20 and SHPP/LPS50 scaffolds with high LPS content were
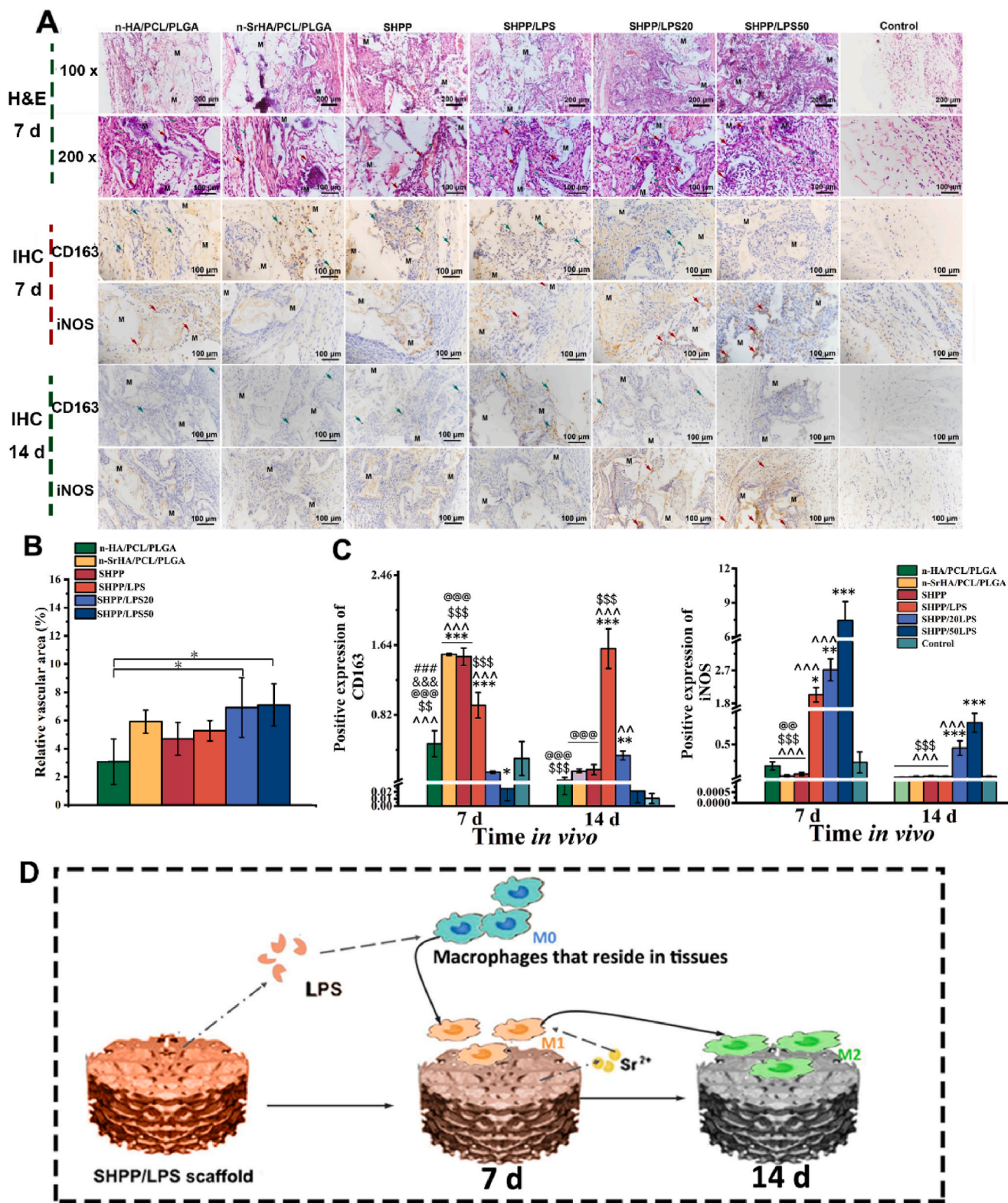
Fig. 7. Images of H&E stained histological sections (red arrows denote the inflammatory cells, green arrows denote the neovascularization) and IHC stained histological sections (CD163: M2 macrophage marker, denoted by green arrows; iNOS: M1 macrophage marker, denoted by red arrows) of scaffolds after subcutaneous implantation for 7 or 14 days (A), M – scaffold material; Semi-quantitative data of relative vascular area in magnified images of H&E stained histological sections of scaffolds after subcutaneous implantation for 7 days (B), n = 5, *P < 0.05, **P < 0.01, ***P < 0.001; Semi-quantitative data of IHC staining (C), * represents comparing with Control, ^ represents comparing with SHPP/LPS50, $ represents comparing with SHPP/LPS20, @ represents comparing with SHPP/LPS, & represents comparing with SHPP, # represents comparing with n-SrHA/PCL/PLGA, n = 4, take * as an example, *P < 0.05, **P < 0.01, ***P < 0.001; Schematic diagram of that SHPP/LPS scaffold induced macrophage homing and polarizing through sequential release of LPS and Sr ions (D). (For interpretation of the references to colour in this figure legend, the reader is referred to the Web version of this article.)

significantly higher than those of the n-HA/PCL/PLGA group (P < 0.05). Although there were no significant differences among the other groups, the mean value of the vascular area in the n-SrHA/PCL/PLGA group was higher than that in the n-HA/PCL/PLGA group and slightly higher than that in the SHPP group, indicating that Sr ion release in the n-SrHA/PCL/PLGA scaffold can play a positive role in promoting angiogenesis. In addition, the mean values of the vascular area in the SHPP, SHPP/LPS, SHPP/LPS20, and SHPP/LPS50 scaffolds showed an increasing trend. There may be at least two reasons for the positive effect of the introduction and concentration elevation of LPS on angiogenesis: 1) the introduction and concentration elevation of LPS in this study facilitated increased infiltration of inflammatory cells, whereas previous studies have shown that the upregulation of angiogenesis and vascular-related factors is associated with inflammation [50,51]; 2) the introduction of LPS could recruit more cells to the scaffold area, interact with the scaffold material, and guide greater phagocytic behavior of inflammatory cells to the scaffold. These interactions can accelerate the degradation of the SHPP scaffold [52], resulting in the release of more Sr ions and thus more effectively promoting angiogenesis.

IHC staining results for CD163 on day 7 (Fig. 7A and C) showed, positive expression is observed in n-HA/PCL/PLGA, n-SrHA/PCL/PLGA and SHPP groups, and relatively higher in the n-SrHA/PCL/PLGA and SHPP groups. There was still certain CD163 expression in the SHPP/LPS group; however, only sporadic CD163 expression was observed in the SHPP/LPS20 group, and no obvious CD163 expression was observed in the SHPP/LPS50 group. The IHC staining results for iNOS at 7 d were opposite to those for CD163. Sporadic iNOS expression was observed in the n-HA/PCL/PLGA group, whereas almost no iNOS expression was observed in the n-SrHA/PCL/PLGA and SHPP groups. With the introduction and concentration increase of LPS, an upward trend in iNOS expression was observed in the scaffolds. The above results suggest that, at 7 days, macrophages in the n-SrHA/PCL/PLGA and SHPP groups were mostly M2 phenotype, whereas in the n-HA/PCL/PLGA group, M1 and M2 phenotype macrophages co-existed, with the majority being of M2 phenotype. This slightly deviated from the results of macrophage polarization in vitro (Fig. 5C and D). This is primarily because the inflammatory response in vivo was a dynamic and gradually fading process [3], and with the fading of inflammation, M1 phenotype macrophages would gradually disappear or transform into M2 phenotype under regulation of biomaterials and body. Further, SHPP/LPS exhibited M1-and M2 phenotypes macrophages simultaneously, and the number of the two phenotypes were close. The macrophages in SHPP/LPS20 group were mostly M1 phenotype. In addition, the number of macrophages in SHPP/LPS50 group increased rapidly and were almost all M1 phenotype.

IHC staining results of CD163 at 14 d (Fig. 7A) showed that, compared with the 7 d results, positive expression in the n-HA/PCL/PLGA, n-SrHA/PCL/PLGA, and SHPP groups decreased sharply, with only sporadic positive expression. Whereas CD163 expression in the SHPP/LPS group was significantly increased, and a large number of positive cells were observed in aggregation. CD163 expression in the SHPP/LPS20 group was slightly increased compared with that 7 d results. In the SHPP/LPS50 group, no obvious CD163 positive expression was observed, similar to the 7 d results. The IHC staining results of iNOS at 14 d showed no significant positive expression of iNOS in the n-HA/PCL/PLGA, n-SrHA/PCL/PLGA, SHPP, and SHPP/LPS groups, while the SHPP/LPS20 and SHPP/LPS50 groups still showed obvious positive iNOS expression. These results suggest that at 14 d, inflammation in most groups gradually subsided, and the number of macrophages decreased overall, except for the SHPP/LPS20 and SHPP/LPS50 groups. Sporadic M2 macrophages were observed in the n-HA/PCL/PLGA, n-SrHA/PCL/PLGA, and SHPP groups. In the SHPP/LPS group, there were still numerous M2 phenotype macrophages, which may be because, as shown in Fig. 7C, M1 phenotype macrophages recruited by LPS in the early stage were transformed into M2 phenotype under the regulation of the scaffold. The macrophages in the SHPP/LPS20 and SHPP/LPS50

groups were mostly of M1 phenotype, suggesting that the stronger inflammatory response caused by the high LPS content was difficult to reverse by the scaffold effect.

All histological evaluation results illustrate that: 1) the n-SrHA/PCL/PLGA and SHPP groups have an optimistic effect on regulating the macrophage phenotype and angiogenesis owing to the presence of Sr ions. (2) The Introduction of LPS recruited more cells infiltration, including macrophages. Pro-inflammatory M1 macrophages recruited by a small amount of LPS (SHPP/LPS scaffold) in the early stage can be reversely regulated by biomaterials at later stages (e.g., day 14) and translocated to pro-regenerative M2 macrophages.

3.9. In vivo osteogenic effects of scaffolds

Fig. 8A and B shows the micro-CT reconstruction images and quantitative BV/TV, Tb.Th and Tb.Sp data after implantation into the femoral condylar defect. At 4 weeks, there was only a small amount of bone formation at the edge of the scaffolds or in the peripheral area of the defects, and no significant difference was observed in the BV/TV, Tb.Th and Tb.Sp value among the groups. At 12 weeks, BV/TV and Tb.Th in all groups were significantly increased, and Tb.Sp was significantly decreased, indicating that new bone formation was observed in all groups, and bone was gradually maturing. Although there was no significant difference observed in Tb.Th and Tb.Sp among all groups, new bone formation in the SHPP/LPS group was better than that in the other groups. More bone tissue grew into the middle area of the scaffold, and its BV/TV value was significantly higher than that in the other groups (P < 0.05). The n-SrHA/PCL/PLGA and SHPP groups also displayed good osteogenic effects, and their BV/TV values were similar and significantly higher than those of the SHPP/LPS50 group (P < 0.05). There was no significant difference in BV/TV values among the remaining groups; however, from the perspective of mean value, the order after the SHPP/LPS group was n-SrHA/PCL/PLGA and SHPP, Control, n-HA/PCL/PLGA, SHPP/LPS20, and SHPP/LPS50.

The images of H&E-stained histological sections (Fig. 8C) showed that all scaffolds maintained good structural integrity at 4 weeks; thus, the defect area in all scaffold groups remained circular (dotted green circles). After 12 weeks, the n-HA/PCL/PLGA and n-SrHA/PCL/PLGA scaffolds deformed severely (green dotted circle), whereas the SHPP and SHPP/LPS scaffolds maintained their initial circular shapes. This is consistent with the in vitro degradation results (Fig. 4) wherein the overall structure of the first two scaffolds significantly shrunk at 12 weeks after degradation, while the SHPP scaffolds maintained their initial shape well. This further proved that the introduction of SrHAW whiskers played an important role in improving the deformation resistance. SHPP/LPS20 and SHPP/LPS50 also showed a certain degree of deformation, which may have been caused by the relatively strong inflammatory response triggered by excessive LPS, and the nibbling effect of inflammatory cells accelerated the scaffold collapse. The enlarged H&E images showed that at 4 weeks, numerous cells, including certain multinucleated macrophages (red arrow), grew into the pore structure of each scaffold. Immature braided bone formation (B, Fig. 8C) was observed in the pore structure of the SHPP/LPS scaffold, whereas no significant bone formation was observed in the other groups. In the control group, a small amount of new bone was observed at the edge of the defect. However, a large amount of loose connective tissue was observed in the middle of the defect area, primarily because of the lack of a block against the peripheral soft tissue. At 12 weeks, all scaffold groups showed a certain amount of new bone formation in the defect area, and the overall trend was consistent with the micro-CT results. In the SHPP/LPS group, the new bone was continuous and clear in outline, and there was almost no unmineralized fibrous tissue, indicating that the mature bone tissue was preliminarily completed. No obvious fibrous tissue was observed at the interface between the new bone and material, indicating that the SHPP/LPS scaffold had good bone integration performance. The SHPP group also formed significant new bones that
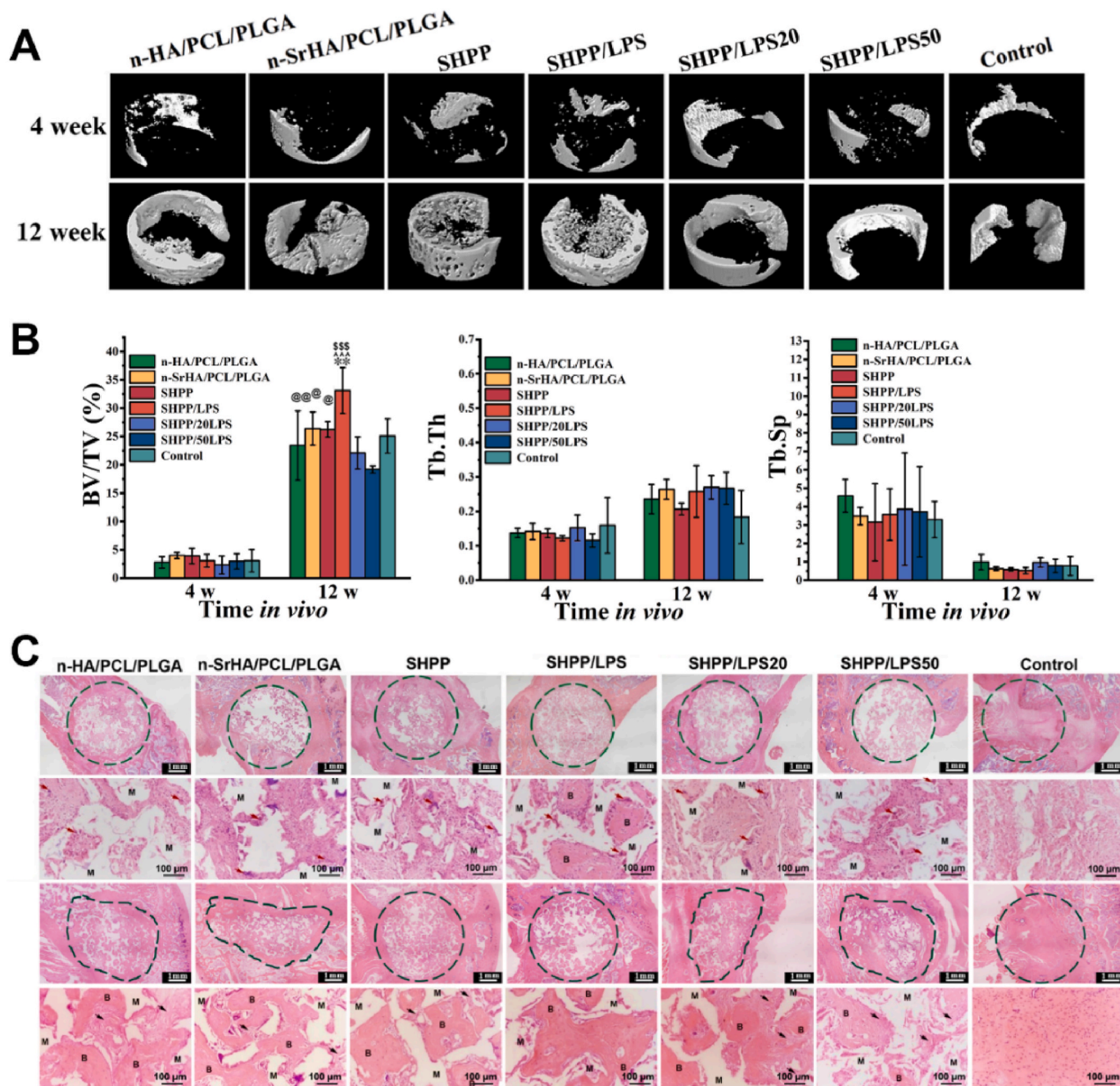
Fig. 8. Micro-CT 3D reconstructed images of new bone tissue (A), and the quantitative BV/TV, Tb.Th, and Tb.Sp value (B) for scaffolds at 4 and 12 weeks after implantation, * represents comparing with Control, ^ represents comparing with SHPP/LPS50, $ represents comparing with SHPP/LPS20, @ represents comparing with SHPP/LPS. n = 3, take * as an example, *P < 0.05, **P < 0.01, ***P < 0.001; The images of H&E stained histological sections of scaffolds after implantation into femoral condyle defects for 4 or 12 weeks (C), the dotted green circle denotes the defect area, M − scaffold material, B - new bone, red arrows denote inflammatory cells, black arrows denote unmineralized fibrous tissue. (For interpretation of the references to colour in this figure legend, the reader is referred to the Web version of this article.)

integrated well with the scaffold; however, a little unmineralized fibrous tissue was observed (black arrow). The bone tissue continuity and maturity were not as good as the SHPP/LPS group. Similar with the SHPP group, the n-SrHA/PCL/PLGA group formed many new bones. However, owing to the narrowing of space caused by the collapse of scaffolds, bone tissue continuity and maturity in the n-SrHA/PCL/PLGA group were inferior to those in the SHPP and SHPP/LPS groups, which indirectly indicates that the SHPP scaffold has a strong ability to maintain structural integrity and effectively maintain the space for bone tissue regeneration and reconstruction. Many new bone formations were also observed in the n-HA/PCL/PLGA group. However, there was more

unmineralized fibrous tissue (black arrow) than in the n-SrHA/PCL/PLGA group. As expected, significantly reduced bone formation and more fibrous tissue were observed in the SHPP/LPS20 group, and the SHPP/LPS50 group performed even worse, indicating that excessive LPS had a negative effect on osteogenesis. At 12 weeks, the control group also displayed certain new bones in the peripheral are; however, a large amount of dense connective tissue differing from the bone tissue was observed in the middle defect area, which may have resulted from the gradual densification of the loose soft tissue invading early.

In vivo osteogenic results demonstrated the following: 1) The osteogenic effect of the n-SrHA/PCL/PLGA, SHPP, and SHPP/LPS scaffolds

with Sr was better than that of n-HA/PCL/PLGA, indicating that the presence of Sr ions can promote bone formation. By comprehensively analyzing all *in vivo* and *in vitro* experiments, Sr ions may contribute to bone formation *in vivo* for two reasons. First, Sr ions promote angiogenesis *in vivo* by polarizing macrophages to M2 phenotype, thus promoting continuous oxygen and nutrient delivery needed by oxidative metabolism during osteogenesis, and indirectly promoting bone regeneration [53]. Second, Sr ions can promote the osteogenic differentiation of osteogenic precursor cells. 2) The gradient degradation endowed by the PCL/PLGA dual matrices, along with the structural integrity maintenance ability endowed by strontium-doped hydroxyapatite whiskers (SrHAW), made the SHPP and SHPP/LPS groups with more continuous bone structure formation. Gradient degradation ensured the continuous release of Ca and Sr ions with osteogenic bioactivity, while avoiding the rapid collapse of the scaffold structure. Moreover, the reinforcement effect of SrHAW endowed the scaffold with a better ability to withstand deformation under stress and *in vivo* environments, which plays an important role in maintaining the growth space of the bone tissue. 3) The introduction of a small amount of LPS had a positive effect on bone formation; therefore, the SHPP/LPS group exhibited the best outcome of bone formation among all groups. By comprehensively analyzing all *in vivo* experiments, it can be concluded that LPS in scaffolds can recruit various cells, including macrophages, to infiltrate and interact with the scaffold at an early stage, thus initializing the tissue repair process as early as possible.

The *in vitro* cell experiments and *in vivo* osteogenic results jointly suggested that although the SHPP and SHPP/LPS scaffolds were inferior to the n-SrHA/PCL/PLGA scaffold *in vitro*, they exhibited better osteogenic effects than the n-SrHA/PCL/PLGA scaffold during *in vivo* implantation. This is because the *in vivo* implantation environment was more complicated than *in vitro* and accelerated the degradation of scaffolds, which provided an opportunity for the release of more Sr and Ca ions, thus improving the efficiency of angiogenesis and osteogenesis *in vivo*. In addition, for the n-SrHA/PCL/PLGA scaffold, owing to the lack of enhancement and toughening effects of SrHAW, the complicated *in vivo* environment resulted in rapid degradation and even structural collapse of the scaffold (Fig. 8C). This, compromised the growth space of the bone tissue, introduced more acidic PLGA products in a short time, and was not conducive for new bone formation.

4. Conclusion

This study developed a composite porous scaffold (SHPP) with progressive degradation by combining Sr-doped micro/nano-hydroxyapatite with PCL/PLGA dual matrices. Additionally, LPS was physically absorbed onto the SHPP composite scaffold to construct an SHPP/LPS scaffold with a sequential immune activation function. The SHPP/LPS scaffold released LPS early to promote macrophage homing in the defect cavity and induce the expression of the pro-inflammatory M1 phenotype. Subsequently, it released Sr ions to suppress inflammation and promote tissue repair. *In vitro* and *in vivo* experiments illustrated that, the SHPP/LPS scaffold's combination of pro-inflammatory effects at the initial stage of implantation, anti-inflammatory effects at a later stage, and structural stability synergistically promoted bone regeneration. The sequential immunomodulatory biomaterial model, represented by the SHPP/LPS scaffold, shows significant potential in bone regeneration and repair, also provides a novel approach for designing future bone repair scaffolds.

CRediT authorship contribution statement

Jinhui Huang: Writing – original draft. **Jiawei Wei:** Methodology, Data curation. **Xue Xia:** Methodology, Data curation. **Shiqi Xiao:** Methodology, Data curation. **Shue Jin:** Methodology. **Qin Zou:** Methodology. **Yi Zuo:** Methodology. **Yubao Li:** Supervision. **Jidong Li:** Writing – review & editing, Conceptualization.

Declaration of competing interest

The authors declare that they have no known competing financial interests or personal relationships that could have appeared to influence the work reported in this paper.

Data availability

Data will be made available on request.

Appendix A. Supplementary data

Supplementary data to this article can be found online at https://doi.org/10.1016/j.mtbio.2024.101063.

References

[1] J. Mao, L. Chen, Z. Cai, S. Qian, Z. Liu, B. Zhao, Y. Zhang, X. Sun, W. Cui, Advanced biomaterials for regulating polarization of macrophages in wound healing, Adv. Funct. Mater. 32 (12) (2021) 2111003.

[2] S. Jin, R. Yang, C. Chu, C. Hu, Q. Zou, Y. Li, Y. Zuo, Y. Man, J. Li, Topological structure of electrospun membrane regulates immune response, angiogenesis and bone regeneration, Acta Biomater. 129 (2021) 148–158.

[3] Z. Julier, A. Park, P. Briquez, M. Martino, Promoting tissue regeneration by modulating the immune system, Acta Biomater. 53 (2017) 13–28.

[4] Y. Wang, H. Zhang, Y. Hu, Y. Jing, Z. Geng, J. Su, Bone repair biomaterials: a perspective from immunomodulation, Adv. Funct. Mater. 32 (51) (2022) 2208639.

[5] L. Chen, L. Zhang, H. Zhang, X. Sun, D. Liu, J. Zhang, Y. Zhang, L. Cheng, H. Santos, W. Cui, Programmable immune activating electrospun fibers for skin regeneration, Bioact. Mater. 6 (10) (2021) 3218–3230.

[6] Y. Liu, T. Segura, Biomaterials-mediated regulation of macrophage cell fate, Front Bioeng Biotech 8 (2020) 609297.

[7] K. Spiller, T. Koh, Macrophage-based therapeutic strategies in regenerative medicine, Adv. Drug Deliv. Rev. 122 (2017) 74–83.

[8] E. Mass, F. Nimmerjahn, K. Kierdorf, A. Schlitzer, Tissue-specific macrophages: how they develop and choreograph tissue biology, Nat. Rev. Immunol. 23 (9) (2023) 563–579.

[9] D. Mosser, J. Edwards, Exploring the full spectrum of macrophage activation, Nat. Rev. Immunol. 8 (12) (2008) 958–969.

[10] T. Wynn, K. Vannella, Macrophages in tissue repair, regeneration, and fibrosis, Immunity 44 (3) (2016) 450–462.

[11] S. Chen, A.F.U.H. Saeed, Q. Liu, Q. Jiang, H. Xu, G.G. Xiao, L. Rao, Y. Duo, Macrophages in immunoregulation and therapeutics, Signal Transduct Tar 8 (1) (2023) 207.

[12] F. Cai, P. Wang, W. Chen, R. Zhao, Y. Liu, The physiological phenomenon and regulation of macrophage polarization in diabetic wound, Mol. Biol. Rep. 50 (11) (2023) 9469–9477.

[13] Z. Lin, D. Shen, W. Zhou, Y. Zheng, T. Kong, X. Liu, S. Wu, P. Chu, Y. Zhao, J. Wu, K. Cheung, K. Yeung, Regulation of extracellular bioactive cations in bone tissue microenvironment induces favorable osteoimmune conditions to accelerate in situ bone regeneration, Bioact. Mater. 6 (8) (2021) 2315–2330.

[14] J. Tan, C. Zhao, Y. Wang, Y. Li, K. Duan, J. Wang, J. Weng, B. Feng, Nano-topographic titanium modulates macrophage response in vitro and in an implant-associated rat infection model, RSC Adv. 6 (113) (2016) 111919–111927.

[15] Z. Tu, Y. Zhong, H. Hu, D. Shao, R. Haag, M. Schirner, J. Lee, B. Sullenger, K. W. Leong, Design of therapeutic biomaterials to control inflammation, Nat. Rev. Mater. 7 (7) (2022) 557–574.

[16] X. Gao, H. Wang, S. Luan, G. Zhou, Biofabrication of poly(aryletherketone)-hydroxyapatite composite scaffolds via low-temperature printing, Adv Mater Technol 8 (8) (2023) 2201676.

[17] Y. Li, Z. Yu, F. Ai, C. Wu, K. Zhou, C. Cao, W. Li, Characterization and evaluation of polycaprolactone/hydroxyapatite composite scaffolds with extra surface morphology by cryogenic printing for bone tissue engineering, Mater Design 205 (2021) 109712.

[18] J. Huang, X. Xia, Q. Zou, J. Ma, S. Jin, J. Li, Y. Zuo, Y. Li, The long-term behaviors and differences in bone reconstruction of three polymer-based scaffolds with different degradability, J. Mater. Chem. B 7 (48) (2019) 7690–7703.

[19] J. Huang, J. Wei, S. Jin, Q. Zou, J. Li, Y. Zuo, Y. Li, The ultralong-term comparison of osteogenic behavior of three scaffolds with different matrices and degradability between one and two years, J. Mater. Chem. B 8 (41) (2020) 9524–9532.

[20] L. Zou, L. Hu, P. Pan, S. Tarafder, M. Du, Y. Geng, G. Xu, L. Chen, J. Chen, C.H. Lee, Icariin-releasing 3D printed scaffold for bone regeneration, Compos Part B-Eng 232 (2022) 109625.

[21] X. Li, Q. Zou, J. Wei, W. Li, The degradation regulation of 3D printed scaffolds for promotion of osteogenesis and in vivo tracking, Compos Part B-Eng 222 (2021) 109084.

[22] H. Zhang, M. Zhang, Effect of surface treatment of hydroxyapatite whiskers on the mechanical properties of bis-GMA-based composites, Biomed Mater 5 (5) (2010) 054106.

[23] W. Choi, H. Kim, M. Kim, U. Kim, J. Kim, Y. Koh, Production and characterization of calcium phosphate (CaP) whisker-reinforced poly(ε-caprolactone) composites as bone regenerative, Mat Sci Eng C 30 (8) (2010) 1280–1284.

[24] J. Huang, X. Xia, Y. Dou, J. Gao, C. Yuan, J.I. Li, J. Wang, Y. Li, Morphology regulation of Sr-substituted hydroxyapatite by l-glutamic acid in a solvent- and initial temperature-dependent manner, Colloid. Surface. 613 (2021) 126117.

[25] X. Sheng, C. Li, Z. Wang, Y. Xu, Y. Sun, W. Zhang, H. Liu, J. Wang, Advanced applications of strontium-containing biomaterials in bone tissue engineering, Mater Today Bio 20 (2023) 100636.

[26] E. O'Neill, G. Awale, L. Daneshmandi, O. Umerah, K. Lo, The roles of ions on bone regeneration, Drug Discov. Today 23 (4) (2018) 879–890.

[27] F. Zhao, B. Lei, X. Li, Y. Mo, R. Wang, D. Chen, X. Chen, Promoting in vivo early angiogenesis with sub-micrometer strontium-contained bioactive microspheres through modulating macrophage phenotypes, Biomaterials 178 (2018) 36–47.

[28] J. Oh, A. Riek, S. Weng, M. Petty, D. Kim, M. Colonna, M. Cella, C. Bernal-Mizrachi, Endoplasmic reticulum stress controls M2 macrophage differentiation and foam cell formation, J. Biol. Chem. 287 (15) (2012) 11629–11641.

[29] A. Rezaei, M. Mohammadi, In vitro study of hydroxyapatite/polycaprolactone (HA/PCL) nanocomposite synthesized by an in situ sol-gel process, Mat Sci Eng C 33 (1) (2013) 390–396.

[30] H. Jscott, Porous scaffold design for tissue engineering, Nat. Mater. 4 (2005) 518–524.

[31] X. Hao, S. Miao, Z. Li, T. Wang, B. Xue, J. Chen, C. Xian, L. Bi, 3D printed structured porous hydrogel promotes osteogenic differentiation of BMSCs, Mater Design 227 (2023) 111729.

[32] K. Cui, Y. Zhang, T. Fu, J. Wang, X. Zhang, Toughening mechanism of mullite matrix composites: a review, Coatings 10 (7) (2020) 672.

[33] H. Zhu, D. Guo, L. Sun, H. Li, D.A. Hanaor, F. Schmidt, K. Xu, Nanostructural insights into the dissolution behavior of Sr-doped hydroxyapatite, J. Eur. Ceram. Soc. 38 (16) (2018) 5554–5562.

[34] Y. Du, J.L. Guo, J. Wang, A.G. Mikos, S. Zhang, Hierarchically designed bone scaffolds: from internal cues to external stimuli, Biomaterials 218 (2019) 119334.

[35] P. Tufekci, A. Tavakoli, C. Dlaska, M. Neumann, M. Shanker, S. Saifzadeh, R. Steck, M. Schuetz, D. Epari, Early mechanical stimulation only permits timely bone healing in sheep, J. Orthop. Res. 36 (6) (2018) 1790–1796.

[36] P. Thevenot, A.M. Nair, J. Shen, P. Lotfi, C.Y. Ko, L. Tang, The effect of incorporation of SDF-1alpha into PLGA scaffolds on stem cell recruitment and the inflammatory response, Biomaterials 31 (14) (2010) 3997–4008.

[37] M.J. Feito, R. Diez-Orejas, M. Cicuendez, L. Casarrubios, J.M. Rojo, M.T. Portoles, Characterization of M1 and M2 polarization phenotypes in peritoneal macrophages

[38] F. McWhorter, T. Wang, P. Nguyen, T. Chung, W.F. Liu, Modulation of macrophage phenotype by cell shape, Proc Natl Acad Sci U S A 110 (43) (2013) 17253–17258.

[39] Z. Liu, J. Zhu, Z. Li, H. Liu, C. Fu, Biomaterial scaffolds regulate macrophage activity to accelerate bone regeneration, Front. Bioeng. Biotechnol. 11 (2023) 1140393.

[40] Q. Wu, L. Hu, R. Yan, J. Shi, H. Gu, Y. Deng, R. Jiang, J. Wen, X. Jiang, Strontium-incorporated bioceramic scaffolds for enhanced osteoporosis bone regeneration, Bone Res 10 (1) (2022) 55.

[41] M. Chen, Y. Zhang, P. Zhou, X. Liu, H. Zhao, X. Zhou, Q. Gu, B. Li, X. Zhu, Q. Shi, Substrate stiffness modulates bone marrow-derived macrophage polarization through NF-kappaB signaling pathway, Bioact. Mater. 5 (4) (2020) 880–890.

[42] R. Sridharan, B. Cavanagh, A. Cameron, D. Kelly, F. O'Brien, Material stiffness influences the polarization state, function and migration mode of macrophages, Acta Biomater. 89 (2019) 47–59.

[43] P. Martin, D.B. Gurevich, Macrophage regulation of angiogenesis in health and disease, Semin. Cell Dev. Biol. 119 (2021) 101–110.

[44] S. Willenborg, T. Lucas, G. van Loo, J.A. Knipper, T. Krieg, I. Haase, B. Brachvogel, M. Hammerschmidt, A. Nagy, N. Ferrara, M. Pasparakis, S.A. Eming, CCR2 recruits an inflammatory macrophage subpopulation critical for angiogenesis in tissue repair, Blood 120 (3) (2012) 613–625.

[45] Z. Wang, Y. Zhao, Y. Zhao, Y. Zhang, X. Yao, R. Hang, Exosomes secreted by macrophages upon copper ion stimulation can promote angiogenesis, Mat Sci Eng C 123 (2021) 111981.

[46] S. An, The emerging role of extracellular Ca(2+) in osteo/odontogenic differentiation and the involvement of intracellular Ca (2+) signaling: from osteoblastic cells to dental pulp cells and odontoblasts, J. Cell. Physiol. 234 (3) (2019) 2169–2193.

[47] S. Meininger, C. Moseke, K. Spatz, E. Marz, C. Blum, A. Ewald, E. Vorndran, Effect of strontium substitution on the material properties and osteogenic potential of 3D powder printed magnesium phosphate scaffolds, Mat Sci Eng C 98 (2019) 1145–1158.

[48] Z. Geng, L. Ji, Z. Li, J. Wang, H. He, Z. Cui, X. Yang, C. Liu, Nano-needle strontium-substituted apatite coating enhances osteoporotic osseointegration through promoting osteogenesis and inhibiting osteoclastogenesis, Bioact. Mater. 6 (4) (2021) 905–915.

[49] R. Villarreal-Leal, G. Healey, B. Corradetti, Biomimetic immunomodulation strategies for effective tissue repair and restoration, Adv. Drug Deliv. Rev. 179 (2021) 113913.

[50] I. Pousa, J. Mate, X. Salcedo-Mora, M. Abreu, R. Moreno-Otero, J. Gisbert, Role of vascular endothelial growth factor and angiopoietin systems in serum of Crohn's disease patients, Inflamm. Bowel Dis. 14 (1) (2008) 61–67.

[51] K. Oikonomou, A. Kapsoritakis, A. Kapsoritaki, A. Manolakis, E. Tiaka, F. Tsiopoulos, I. Tsiompanidis, S. Potamianos, Angiogenin, angiopoietin-1, angiopoietin-2, and endostatin serum levels in inflammatory bowel disease, Inflamm. Bowel Dis. 17 (4) (2011) 963–970.

[52] Z. Cai, Q. Saiding, L. Cheng, L. Zhang, Z. Wang, F. Wang, X. Chen, G. Chen, L. Deng, W. Cui, Capturing dynamic biological signals via bio-mimicking hydrogel for precise remodeling of soft tissue, Bioact. Mater. 6 (12) (2021) 4506–4516.

[53] R. Riddle, T. Clemens, Bone cell bioenergetics and skeletal energy homeostasis, Physiol. Rev. 97 (2) (2017) 667–698.